Rolling Bearing Fault Diagnosis Based on MResNet-LSTM

Yuanpeng Feng and Zhansi Jiang

School of Naval Architecture and Ocean Engineering, Guangzhou Maritime University, Guangzhou, 510725, China.
School of Mechanical and Electrical Engineering, Guilin University of Electronic Technology, Guilin, 541004, China. E-mail: jiangzhansi@gzmtu.edu.cn

Zhenyu Tang

School of Naval Architecture and Ocean Engineering, Guangzhou Maritime University, Guangzhou, 510725,China.

Yixian Du

Guangdong Provincial Key Laboratory of Intelligent Lithium Battery Manufacturing Equipment, Guangzhou, 510725, China.
Guangdong Lyric Robot Automation Co., Ltd, Guangzhou, 510725, China.

(Received 10 October 2023; accepted 10 March 2024)

In response to the challenges of weak fault characteristics and complex and variable working conditions of roll-ing bearings in strong noise environments, a diagnostic methodology is proposed. This method integrates a multi-scale residual neural network (MResNet) and a long short-term memory (LSTM) neural network to achieve fault diagnosis of bearings under both constant and variable rotational speed working conditions. First, complete an ensemble empirical mode decomposition with adaptive noise (CEEMDAN) that is applied for vibration signal denoising. Secondly, a dropout layer is introduced between multi-scale residual blocks to prevent net-work overfitting, and the powerful time series information capture ability of LSTM is combined to improve di-agnostic accuracy. Finally, experimental verification is conducted using constant and variable speed bearing data sets. The results show that the proposed approach maintains strong diagnostic capabilities when the rotat-ing speed conditions change, and the signal is heavily polluted by noise.

1. INTRODUCTION

Rolling bearings are fundamental components in mechanical systems. In the application fields of rail transit, aerospace, etc., the operational circumstances of bearings are intricate and subject to variations, which makes them become fault-prone parts. If mechanical faults cannot be diagnosed in a timely manner, it could cause unpredictable damage to human safety.[1] Therefore, applying fault diagnosis with rolling bearings holds significant practical importance for safeguarding lives and property, as well as the efficiency of mechanical equipment.[2] In the actual production process, rolling bearings have two operating conditions: constant speed and variable speed. The feature extraction and fault classification are pivotal aspects of bearing fault diagnosis methods that rely on the analysis of vibration signals. The mainstream feature extraction methods, such as wavelet transform,[3] empirical mode decomposition4, and short time Fourier transform,[5] rely more on expertise. Traditional classifiers, such as support vector machines,[6] and artificial neural networks,[7] have low fault recognition rates due to their shallow network structure. In addition, the changes in bearing speed make the collected signal sources exhibit significant non-stationary characteristics, making it difficult for traditional bearing fault diagnosis methods to identify fault types. For variable speed problems, signal processing tech-niques are used in detecting faults in variable speed situations.[8–11] The Computed Order Track (COT) method, which resamples a variable-speed vibration signal into a smooth signal in the angular domain, is a commonly used method for processing variable-speed signals.[12]

In recent years, Convolutional Neural Networks (CNNs) have garnered significant favor among scholars in the field of fault diagnosis. In 2016, CNN began to be used for bearing fault diagnosis.[13] Zhang et al.[14] proposed a convolutional neural network with training interference (TICNN) to solve the problem of machine workload changes and noise in the real industrial environment. Shallow CNN networks may not be able to capture complex features and patterns, and the stacking of layers in CNN networks can cause gradient vanishing or exploding problems. Therefore, Zhao et al.[15] utilizes a deep residual contraction network to address the issues of gradient vanishing or exploding in deep networks. By inserting soft thresholds into the deep architecture, noise related features are eliminated, and strong background noise fault diagnosis is achieved. Zhi et al.[16] suppressed the noise in the sensor data by combining the wavelet region correlation threshold, extracted the data features using CNN, and combined with the powerful time series data processing capability of LSTM to achieve a harmonic reducer fault detection.

Bearing vibration signals can represent different features at different time scales, and using multi-scale networks can capture features of different scales and frequencies.[17] Pan et al.[18]

proposed a novel deep learning network capa-ble of adaptively learning features from raw mechanical data, eliminating the need for prior domain knowledge. Zhao et al.[19] used the multi-scale module with an attention mechanism to build a shared feature generator, and formed a deep multi-scale adversary neural network with a differential discriminator, and verified that the network has excellent diagnostic performance. Wang et al.[20] proposed an innovative approach to fuse multi-modal sensor signals and applied 1D CNN to extract features from raw vibration signals and acoustic signals which subsequently enhanced the precision of bearing fault diagnosis through feature fusion. Huang et al.[17] added the channel attention mechanism to the multi-scale CNN, and extracted the multi-scale information of the signal through the maximum and average pooling layers to achieve bearing fault diagnosis under noise environment and different operating speeds. Liu et al.[21] combined sparse wavelet decomposition with multi-scale neural networks, significantly improving diagnostic accuracy. Qi et al.[22] combined EMD and multi-scale CNN, and re-extracted rich complementary features using the pyramid pool module for bearing fault label assessment.

The above CNN model has achieved good diagnostic results in bearing fault diagnosis, but it is only applicable to the condition of constant bearing speed and cannot achieve bearing fault diagnosis under changing speed conditions. In reality, the operating environment of mechanical equipment can also be mixed with a large amount of noise, thereby reducing the precision of fault diagnosis. To address the aforementioned issues, this paper presents a fault diagnosis methodology that combines a Multi-Scale Residual Network with LSTM (MResNet-LSTM). This method performs angular domain transformation on the vibration signal of variable speed bearings through COT, denoises the fault signal using CEEMDAN, and discards some redundant information in the network by introducing a dropout layer between residual blocks to prevent overfitting and improve diagnostic efficiency. It utilizes convolutional kernels of different sizes to extract richer features and use residual structures to solve the problem of gradient explosion in the model. The method proposed in this paper enables adaptive feature extraction and end-to-end diagnosis of rolling bearings under constant and variable speed operating conditions in the presence of noise interference.

2. BASIC PRINCIPLES

2.1. Long Short-Term Memory Network (LSMN)

LSTM is a special Recurrent Neural Network (RNN) circulatory structure, originally introduced by Hochreiter and Schmidhuber in the late 1990s.[23] LSTM mainly solves the long-term dependency problem of RNN, including forgetting gates, input gates, and output gates. The structural schematic diagram is shown in Fig. 1.

2.2. The Basic Principles Of CEEMDAN

CEEMDAN[24] is proposed on the basis of Set Empirical Mode Decomposition (EEMD), which effectively solves the modal aliasing phenomenon in EEMD. The steps for CEEMDAN are as follows:

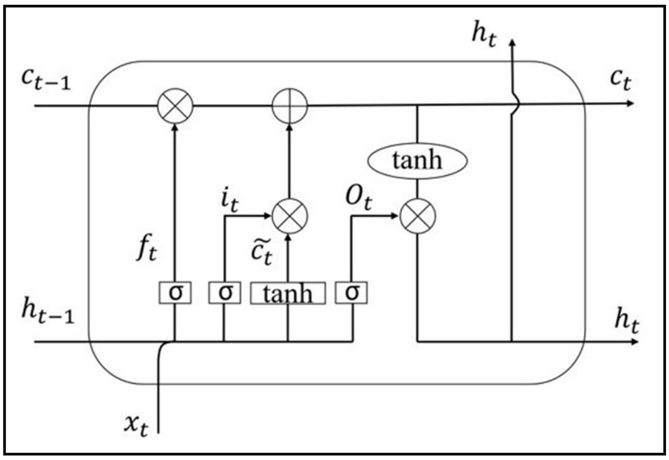

Figure 1. Structure Diagram of LSTM.

Step 1: Introduce Gaussian white noise $\delta_i(t)$ with a normal distribution into the signal $x(t)$ that is to be decom-posed, and construct N times of sequence to be decomposed $x_i(t)$. Where $i = 1, 2, 3, \ldots, N$.

$$x_i(t) = x(t) + \varepsilon\delta_i(t). \tag{1}$$

Step 2: Perform EMD decomposition on the above sequence, take the first mode for mean calculation, and obtain the first order modal component of CEEMDAN.

$$IMF_1 = \frac{1}{N}\sum_{i=1}^{N} IMF_1^i(t). \tag{2}$$

Calculate the first residual component.

$$r_1(t) = x(t) - IMF_1(t). \tag{3}$$

Step 3: Introduce Gaussian white noise to $r_1(t)$ and apply EMD decomposition to the new signal $r_{j-1}(t) + \varepsilon_{j-1}E_{j-1}(\delta_i(t))$ to extract the second-order modal component in CEEMDAN.

$$IMF_2(t) = \frac{1}{N}\sum_{i=1}^{N} E_1(r_1(t) + \varepsilon_1 E_1(\delta_i(t))). \tag{4}$$

Calculate the second residual component.

$$r_2(t) = r_1(t) - IMF_2(t); \tag{5}$$

Step 4: Repeat step 3 to obtain the jth modal component.

$$IMF_j(t) = \frac{1}{N}\sum_{i=1}^{N} E_1(r_{j-1}(t) + \varepsilon_{j-1}E_{j-1}(\delta_i(t))). \tag{6}$$

$$r_j(t) = r_{j-1}(t) - IMF_j(t). \tag{7}$$

Step 5: When the residual component $r_n(t)$ is a monotonic signal, the iteration stops and the decomposition of the CEEMDAN algorithm ends.

2.3. CEEMDAN Denoising Process

This article uses the CEEMDAN denoising flowchart as shown in Fig. 2. The signal with noise is decomposed in-to multiple IMF components through CEEMDAN. Subsequently, the autocorrelation coefficients of each component are calculated. Components with autocorrelation coefficients greater than 0.2 are reconstructed.

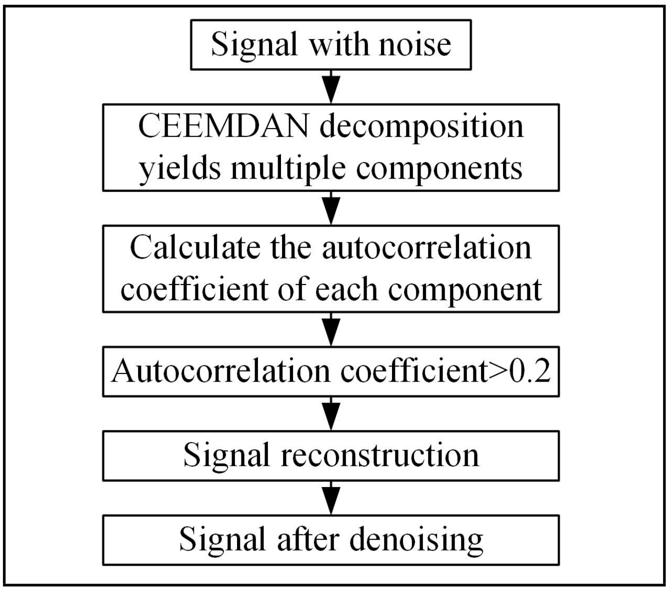

Figure 2. Noise Removal Flow Chart of CEEMDAN.

2.4. Computed Order Track

Computed order track assumes that its reference axis has a constant speed for a period of time. The angle θ of the axis can be described by the following quadratic equation:

$$\theta(t) = b_0 + b_1 t + b_2 t^2. \tag{8}$$

The coefficients b_0, b_1 and b_2 in the formula are the coefficients to be solved, which are determined by fitting the arrival time (t_1, t_2, t_3) of three consecutive key phasors and the axial angle change value $\Delta\phi$.

The following equation system can be established:

$$\begin{cases} \theta(t_1) = 0 \\ \theta(t_2) = \Delta\phi \\ \theta(t_3) = 2\Delta\phi \end{cases}. \tag{9}$$

Substituting Eq. (9) into Eq. (8) yields:

$$\begin{pmatrix} 0 \\ \Delta\phi \\ 2\Delta\phi \end{pmatrix} = \begin{bmatrix} 1 & t_1 & t_1^2 \\ 1 & t_2 & t_2^2 \\ 1 & t_3 & t_3^2 \end{bmatrix} \begin{Bmatrix} b_0 \\ b_1 \\ b_2 \end{Bmatrix}. \tag{10}$$

Once the coefficients b_0, b_1 and b_2 Confirm to obtain:

$$t = \frac{1}{2b_2}[\sqrt{4b_2(\theta - b_0) + b_1^2} - b_1]. \tag{11}$$

Once the time of resampling is determined, the corresponding amplitude of the signal can be calculated by cubic spline interpolation.

3. FAULT DIAGNOSIS MODEL BASED ON MRESNET-LSTM

3.1. Improving Residual Structure

The traditional residual structure, as shown in Fig. 3 (a), is prone to overfitting when the network is stacked with too many layers. The ResNet structure is shown in Fig. 3 (b), a dropout layer is introduced between residual blocks to alleviate overfitting. Each residual block includes three convolutional layers,

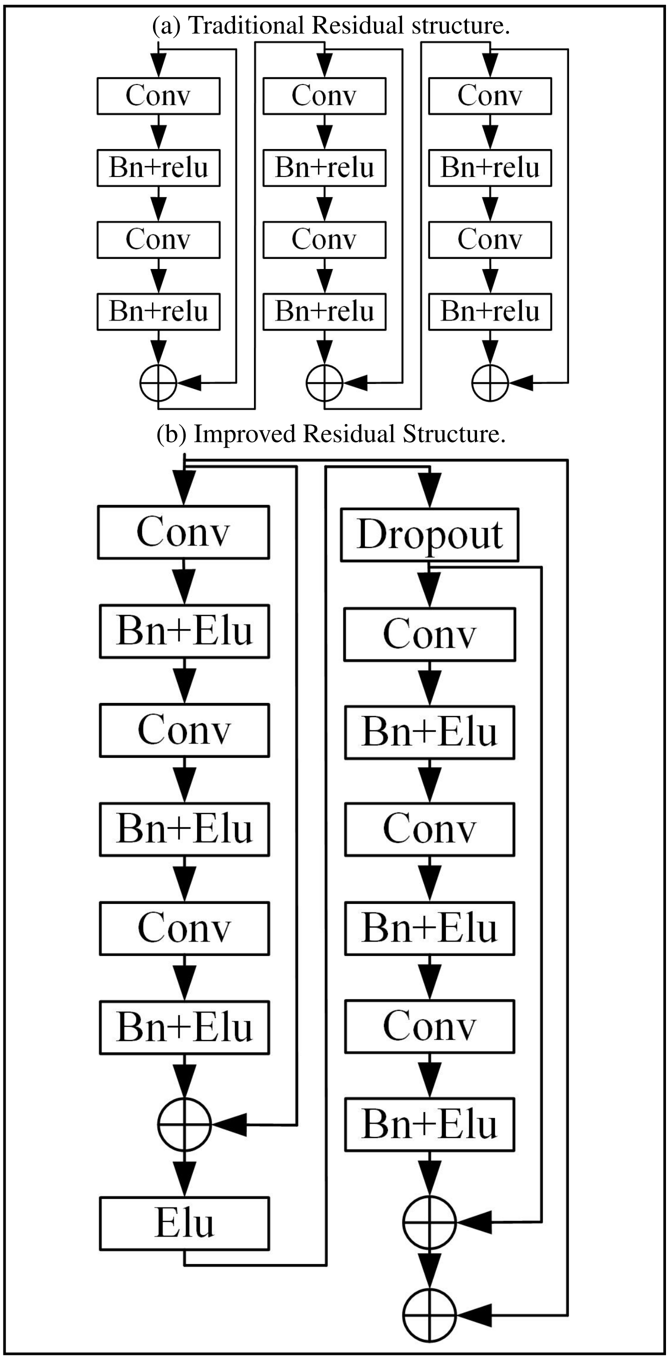

Figure 3. Structure Diagram of Improved ResNet.

BN layers, and activation layers, Utiliz-ing Elu as the activation function. Compared with relu, the output mean value of Elu approximates zero and offers a faster rate of convergence.

$$Elu(x) = \begin{Bmatrix} x, x > 0 \\ \alpha(e^x - 1), x \leq 0 \end{Bmatrix}. \tag{12}$$

3.2. MResNet-LSTM Model

In order to extract deep feature information of different scales from the original vibration signal and prevent gradi-ent vanishing due to the increase of network layers. This article combines the powerful feature extraction ability of multi-scale ResNet and the advantages of LSTM in capturing temporal information of fault occurrence and proposes MResNet-LSTM. The structure diagram of MResNet-LSTM is shown in Fig. 4.

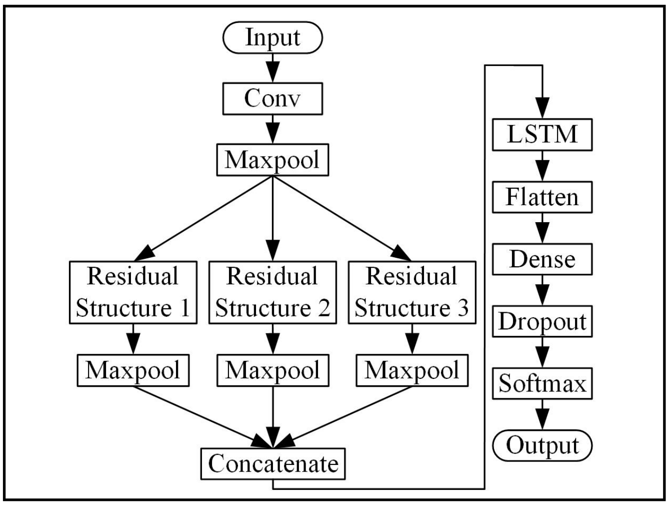

Figure 4. Structure Diagram of MResNet-LSTM.

The network structure includes an initial convolutional layer, a pooling layer, an MResNet layer, a pooling layer, a feature fusion layer, an LSTM layer, an unfolding layer, a fully connected layer, a dropout layer, and a classification layer.

3.3. MResNet-LSTM Fault Diagnosis Process

In response to loud noises in the working environment of rotating machinery, the collected vibration signals of rolling bearings mix with the loud noise and the feature extraction is not sufficient resulting in proposing a MResNet-LSTM network for rolling bearing fault diagnosis. Figure 5 shows the fault diagnosis flowchart. The fault diagnosis process based on MResNet-LSTM is as follows:

1. For bearing vibration signals during constant-speed operation, to simulate the real-work environment, Gaussian white noise is added to vibration signal, followed by denoising using CEEMDAN.

2. For bearing vibration signals under variable speed conditions, Gaussian white noise was added to the vibration signals in order to simulate the actual operating environment. The vibration signal is resampled into angular domain signals using COT and then denoised using CEEMDAN for diagonal domain signals.

3. Divide the denoised signal into a training set, a validation set, and a testing set, and then perform unique hot coding labeling processing.

4. The training set trains the neural network, extracts feature information from the model, and learns fault features.

5. The validation set is used to fine tune model parameters, and after training, a fault diagnosis model can be obtained.

6. The fault diagnosis process is completed by utilizing the test set as input to the model and outputting the fault diagno-sis results.

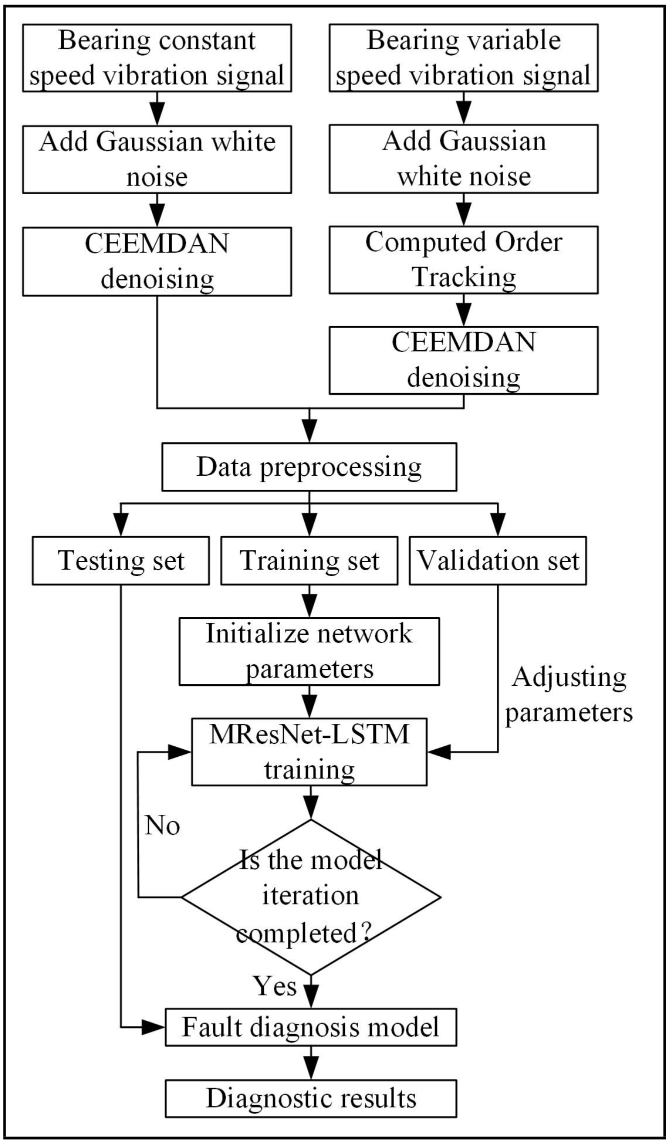

Figure 5. Fault Diagnosis Flow Chart of MResNet-LSTM.

4. EXPERIMENTAL VERIFICATION AND RESULT ANALYSIS

4.1. Fault Diagnosis Of Constant Speed Bearings

4.1.1. Experimental design and data acquisition

The test bench used for this experiment is Spectra Quest Co's Mechanical Fault Simulator (MFS), as shown in Fig. 6. It primarily consists of a signal acquisition and speed control software system, a drive motor, a tachometer, an acceleration sensor and a fault bearing. The type of faulty bearing is ER-12K. Under constant speed conditions, the sampling frequency for testing bearings is set to 12.8 kHz. The bearings are faulty in the inner ring, rolling element, and outer ring, respectively. Under each fault state, they are also in the rotating frequency of 19.88 Hz, 29.87 Hz, and 39.84 Hz. There are a total of 10 different types of bearings available which include bearings under normal conditions.

The fault types and codes of bearings under constant speed operating conditions are shown in Tab. 1. Each type of faulty bearing has 327680 sampling points, with a sample length of 1024. Each type of faulty bearing can be divid-ed into 320

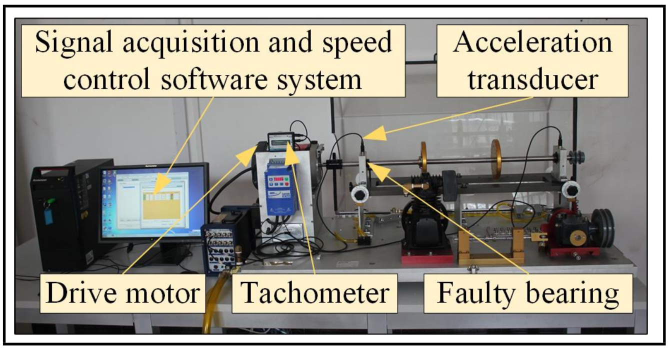

Figure 6. Device Diagram of Bearing Experimental Platform.

Table 1. Fault Types and Codes of Constant Speed Bearings.

Fault type	Rotating frequency	Tags
Normal	19.88 Hz	0
Rolling element fault	19.87 Hz	1
Rolling element fault	29.86 Hz	2
Rolling element fault	39.84 Hz	3
Inner ring failure	19.89 Hz	4
Inner ring failure	29.87 Hz	5
Inner ring failure	39.85 Hz	6
Outer ring fault	19.86 Hz	7
Outer ring fault	29.84 Hz	8
Outer ring fault	39.82 Hz	9

Table 2. Test Results of Dropout Rate for Different Dropouts.

Dropout drop rates	0.1	0.25	0.35	0.5
Accuracy (%)	99.22	99.41	99.25	99.10

samples, totaling 3200 data samples.

4.1.2. Experimental parameter settings

Split the dataset samples into training, validation, and testing sets using a 70 %, 20 %, and 10 % ratio, respectively. In the experiment, the optimizer uses Adam, the learning rate is set to 0.005, the decay rate is 0.01, the activation function of the classification layer uses softmax, and the training batch size is 64.

For the improved residual structure in Fig. 3 (b), the dropout layer randomly discards neurons in the network in a certain proportion, giving less chance for abnormal data with lower probability to learn. Setting the dropout rate too low will limit its effectiveness, while setting it too high will significantly reduce the output features, resulting in insufficient training. This article sets the dropout rates in the improved residual structure to 0.1, 0.25, 0.35 and 0.5, and veri-fies the impact of dropout rates on diagnostic accuracy using the MResNet-LSTM model. The results are shown in Tab. 2, with accuracy representing the mean value from 10 tests. As observed in Tab. 2, the diagnostic accuracy reaches its peak at a dropout rate of 0.25, which is the highest. Consequently, the dropout layer in the improved residual structure adopts a discard rate of 0.25.

For bearing fault diagnosis under constant speed conditions, the model's parameters, are detailed in Tab. 3. The pooling technique employed is maximum pooling, and the activation function utilized is ELU.

4.1.3. Experimental results

The accuracy and loss of the training and validation sets for bearings under constant speed conditions are depicted in Fig. 7.

Table 3. Model Parameters of MResNet-LSTM.

Network structure	Kernel size/stride	Kernel channel size	Number of units
Convolution	64/16	64	—
Pooling 1	2/2	—	—
Residual structure 1	3/1	64	—
Residual structure 2	5/1	64	—
Residual structure 3	7/1	64	—
Pooling 2	9/9	—	—
Feature fusion	—	—	—
LSTM	—	—	64
Fully-connected	—	—	
Dropout	—	—	0.25
Softmax	—	—	10

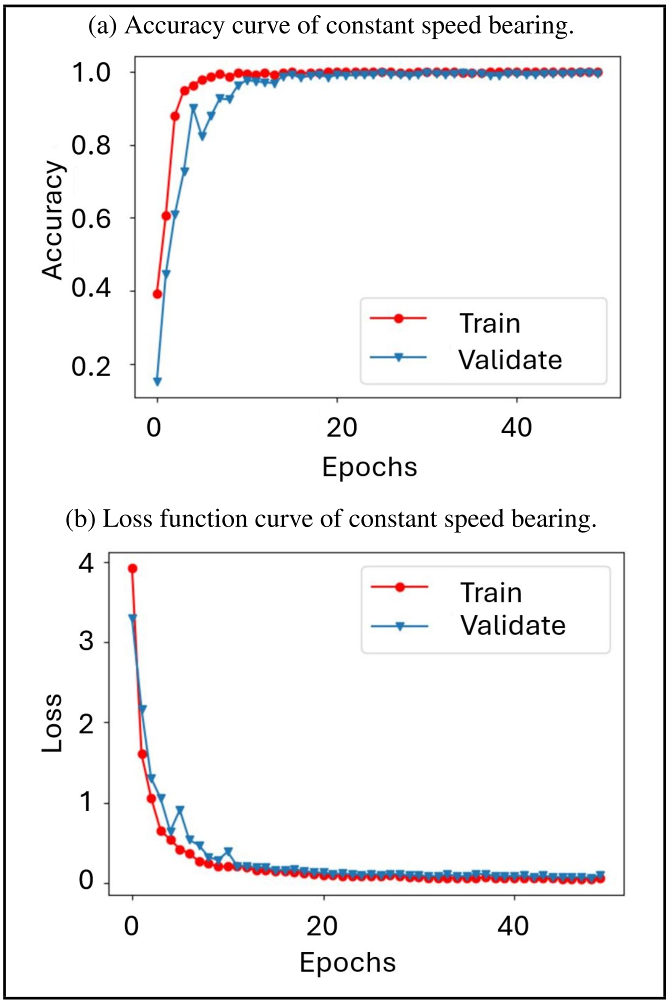

Figure 7. Results of Constant Speed Bearing in the Training Set and Verification Set.

After 20 iterations of the model, both the accuracy of the training and validation sets approaches 100 %, and the loss value remains relatively stable, indicating that the model has converged.

To clarify the recognition effect of the model on various faults in the test set, the confusion matrix is utilized to visualize the test set results, as shown in Fig. 8. The predicted results of MResNet-LSTM for bearings are basically consistent with the label. Under constant speed conditions, diagnostic errors only occurred for rolling element faults with a rotational frequency of 29.86 Hz.

Using t-SNE[25] to demonstrate the feature learning ability of MResNet-LSTM on bearing fault datasets, as shown in Fig. 9, Figs. 9 (a) and (b), the bearing data in the original state is very

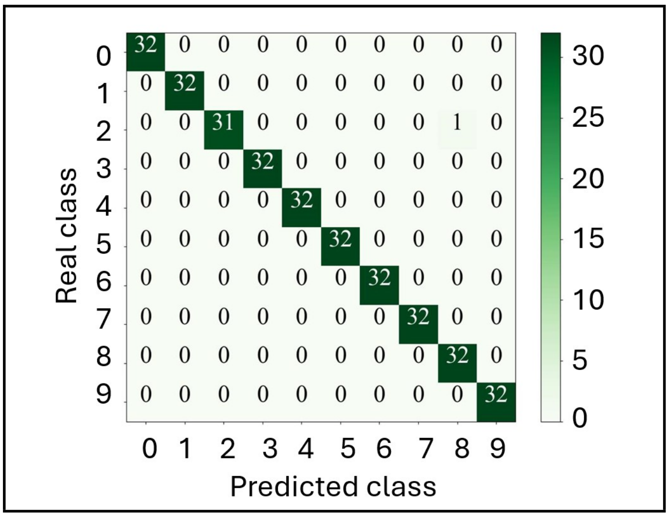

Figure 8. Confusion Matrix of Constant Speed Bearing.

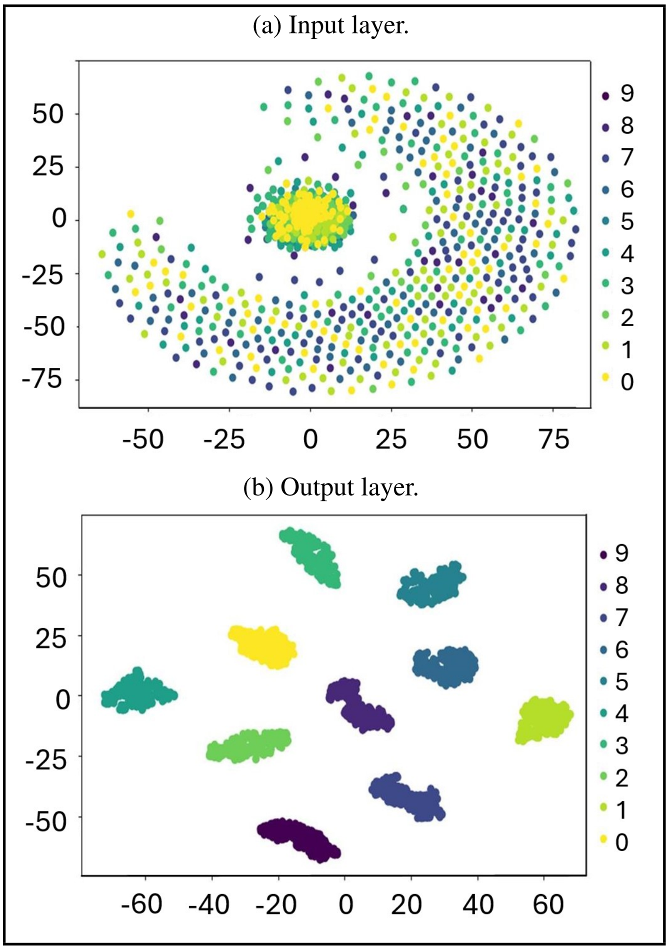

Figure 9. T-SNE Visualization Results of Constant Speed Bearing.

chaotic, with various types of mixed data and is difficult to distinguish. In the output layer, 10 samples were perfectly separated, and samples of the same type were perfectly clustered, indicating that the model has strong feature extraction ability.

4.1.4. Comparative experiment

To verify the effectiveness of MResNet-LSTM, compare it with other different methods. The specific comparison method is as follows: WKCNN,[26] WDCNN,[27] CNN,[28] ResNet-18.[29]

Table 4 shows the experimental results, where the accuracy is the average of 5 tests. As can be seen from Tab. 4, the average accuracy of MResNet-LSTM reaches 99.41 % under the constant speed condition, which exceeds the other comparison methods.

Table 4. Diagnostic accuracy of different methods of constant speed bearing (100 %).

Methods	Average accuracy
WKCNN	98.22
WDCNN	99.1
CNN	98.91
ResNet-18	98.5
Proposed Method	99.41

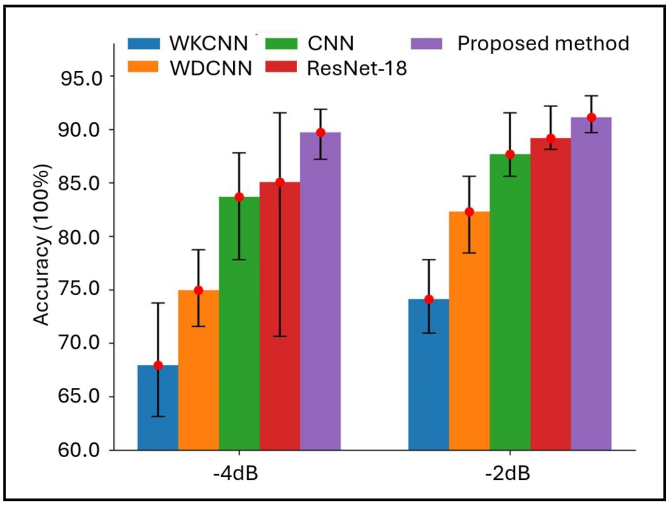

Figure 10. Diagnostic Accuracy of Different Methods for Constant Speed Bearings in Noise Environments.

4.1.5. Analysis of noise resistance performance

To verify the noise resistance performance of MResNet-LSTM, signal-to-noise ratios were set to -4 dB and -2 dB, respectively. Compared with four methods mentioned above, the classification accuracy was the average of 5 tests, as shown in Fig. 10.

As shown in Fig. 11, the accuracy of fault diagnosis has decreased due to noise interference. In the case of signal-to-noise ratios of -4 dB and -2 dB, the average diagnostic accuracy of the MResNet-LSTM model for constant speed bearings is still 89.72 % and 91.13 %, which is higher than other comparison methods. The stability of the five test results is also better than other comparative methods.

4.2. Fault Diagnosis Of Variable Speed Bearings

4.2.1. Experimental design and data acquisition

The fault diagnosis experimental device for variable speed bearings is the same as that for constant speed bearings, using Spectra Quest Co's Mechanical Fault Simulator (MFS). Three vibration signals of variable speed bearings, namely outer ring fault, inner ring fault, and roller fault, were collected in the laboratory. The sampling frequency is 25.6 kHz, and the rotation frequency increases from 0 to 40 Hz. Table 3 displays the fault types and codes of bearings during variable speed operating conditions. Each type of faulty bearing has 360448 sampling points, with a sample length of 1024. Each type of faulty bearing can be divided into 320 samples, totaling 960 data samples.

Table 5. Fault Types and Coding of Variable Speed Bearings.

Fault type	Rotating frequency	Tags
Rolling element fault	0-40Hz	0
Inner ring failure	0-40Hz	1
Outer ring fault	0-40Hz	2

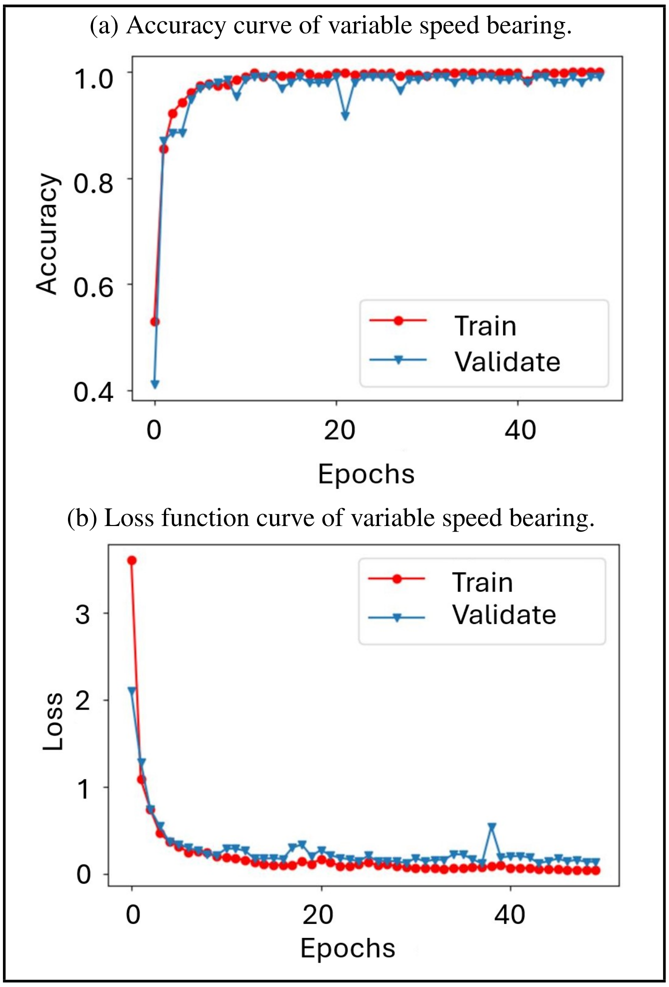

Figure 11. Results of Variable Speed Bearing in Training Set and Verification Set.

4.2.2. Experimental parameter settings

Split the dataset samples into training, validation, and testing sets using a 70 %, 20 %, and 10 % ratio, respectively. In the experiment, the optimizer is set to use Adam, the learning rate is set to 0.005, the decay rate is 0.01, the activation function of the classification layer uses softmax, and the training batch size is 24. Table 5 shown the fault types and codes of bearings under variable speed operating conditions.

4.2.3. Experimental results

The accuracy and loss of the training and validation sets for bearings under variable speed conditions are depicted in Fig. 11, with both the accuracy of the training and validation sets approaching 100 %.

To clarify the identification effect of the model on various faults in the variable speed fault bearing test set, the Confusion matrix is used to visualize the results of the test set. As shown in Fig. 12, the prediction results of MRes-Net-LSTM on bearings are basically consistent with the labels. Under variable speed conditions, diagnostic errors only occur for outer ring faults.

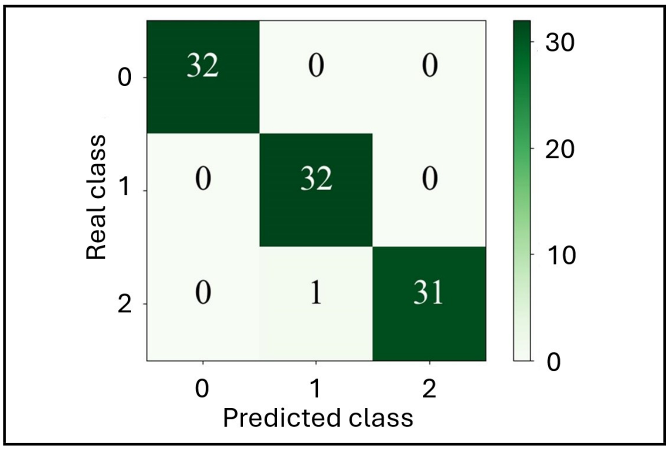

Figure 12. Confusion Matrix of Variable Speed Bearing.

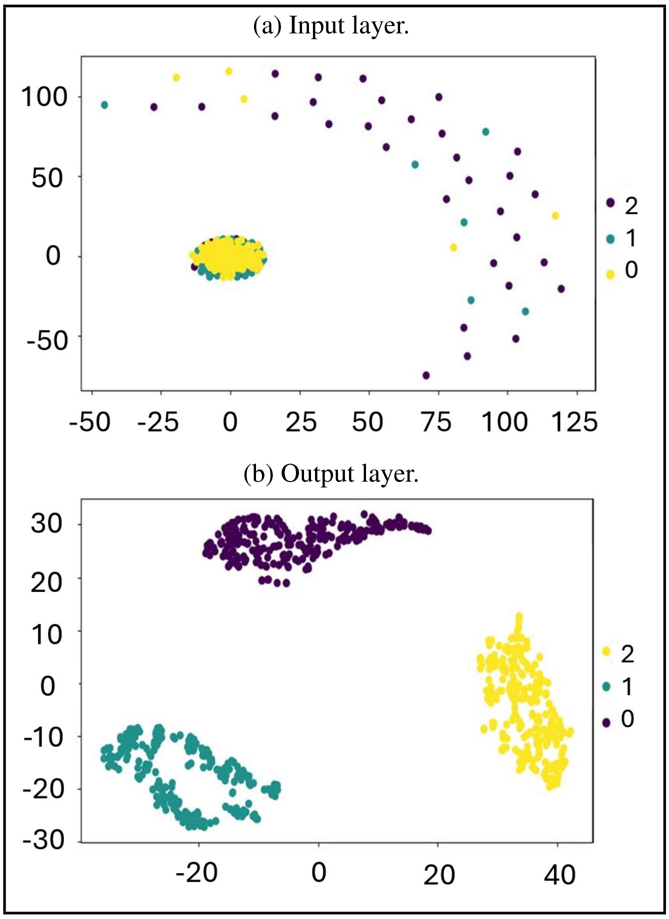

Figure 13. Results of Variable Speed Bearing in Training Set and Verification Set.

Using t-SNE to demonstrate the feature learning ability of MResNet-LSTM on variable speed bearing fault datasets are shown in Fig. 13. From Figs. 13 (a) and (b), it can be seen that various types of data present a chaotic state in the input layer, while the three fault types are perfectly separated in the output layer. This model has strong feature extraction ability for variable speed bearing fault data.

4.2.4. Comparative experiment

To verify the effectiveness of MResNet-LSTM, corner domain signals were used as inputs, and MResNet-LSTM was compared with the four methods mentioned above. Mean-

Table 6. Diagnostic Accuracy of Variable Speed Bearings Using Different Methods (100 %)

Methods	Average accuracy
WKCNN	97.71
WDCNN	97.5
CNN	97.29
ResNet-18	96.46
MResNet-LSTM (Input vibration signal)	88.75
Proposed Method	98.44

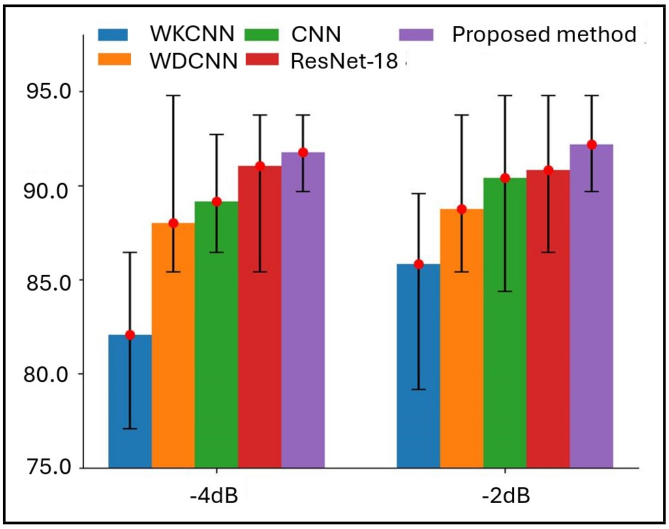

Figure 14. Accuracy of different methods for variable speed bearings in noise environments.

while, verification of the effectiveness of resampling variable speed signals were completed using computational order tracking. The comparison method was added using vibration signals as input to MResNet-LSTM. Table 6 shows the results where the accuracy is the average of 5 tests. In Tab. 6, it is evident that the computed order track and resampling of the variable speed bearing vibration signal into an angular domain signal as input data, the diagnostic accuracy of the network can be improved. Using angular domain signals as input to the MResNet-LSTM model, the average diagnostic accuracy reaches 98.44 % under varia-ble speed conditions, which is higher than other comparison methods.

4.2.5. Analysis of noise resistance performance

To verify the noise resistance of MResNet-LSTM under variable speed conditions, the signal-to-noise ratios were also set to -4 dB and -2 dB, respectively. Compared with four methods mentioned above, the classification accuracy was the average of 5 tests, as shown in Fig. 14.

As shown in Fig. 14, MResNet-LSTM has an average diagnostic accuracy of 91.77 % and 92.92 % for variable speed bearings at a signal-to-noise ratio of -4 dB and -2 dB, respectively, which is superior to other comparison methods.

5. CONCLUSIONS

When addressing the challenge of effectively diagnosing rolling bearing faults in strong-noise environments, a method employing MResNet-LSTM for bearing fault diagnosis was proposed. This approach combines the strong feature extraction capabilities of the multi-scale residual network with the time series analysis capabilities of LSTM. It enables fault diagnosis under both constant and variable speed conditions, while also demonstrating robust anti-interference performance. The analysis leads to the following conclusions:

1. The diagnostic method combining multi-scale ResNet and LSTM was validated on a constant speed bearing dataset. The average diagnostic accuracy of the test set in the experiment reached 99.41 %. Furthermore, on the variable speed condition bearing dataset, the average diagnostic accuracy achieved 98.44 %.

2. This model still maintains high diagnostic accuracy even in the presence of strong noise in vibration signals, effectively reducing the impact of noise on identification results.

3. By adding a dropout layer between residual blocks to remove redundant information in the network, overfitting is prevented, diagnostic efficiency is improved, and the model's generalization ability is enhanced.

ACKNOWLEDGEMENTS

This project was supported by Guangdong Provincial Key Laboratory of Intelligent Lithium Battery Manufactur-ing Equipment (2022B1212020003), AI Enabled Production Lifecycle Management for Flexible HMC (2022YFE0114100), Guangzhou Quality Engineering Project (2023YLKC034), Guangdong Provincial Characteristic Innovation Project (2019KTSCX126), and Innovation Project of Guangxi Graduate Education (YCBZ2023135). Innovation Project of GUET Graduate Education (2023YCXS017).

REFERENCES

[1] Wang R, Jiang H, Zhu K, Wang Y, Liu C. A deep feature enhanced reinforcement learning method for rolling bearing fault diagnosis, *Advanced Engineering Informatics*, **54**, 101750, (2022). https://doi.org/10.1016/j.aei.2022.101750

[2] Hu X, Man J, Yang H, Deng J, Liu Y. An Improved Metalearning Framework to Optimize Bearing Fault Diagno-sis under Data Imbalance, *Journal of Sensors*, **2022**, 1809482, (2022). https://doi.org/10.1155/2022/1809482

[3] Li W, Cao Y, Li L, Hou S. Orthogonal Wavelet Transform-Based Gaussian Mixture Model for Bearing Fault Diagnosis, *Discrete Dynamics in Nature and Society*, **2023**, 1307845, (2023). https://doi.org/10.1155/2023/1307845

[4] Meng D, Wang H, Yang S, Lv Z, Hu Z, Wang Z. Fault Analysis of Wind Power Rolling Bearing Based on EMD Feature Extraction, *Computer Modeling in Engineering & Sciences*, **130**, 543-558, (2022). https://doi.org/10.32604/cmes.2022.018123

[5] Jiang Z, Zhang K, Xiang L, Yu G, Xu Y. A time-frequency spectral amplitude modulation method and its appli-cations in rolling bearing fault diagnosis, *Mechanical Systems and Signal Processing*, **185**, 109832, (2023). https://doi.org/10.1016/j.ymssp.2022.109832

[6] Zhou J, Xiao M, Niu Y, Ji G. Rolling Bearing Fault Diagnosis Based on WGWOA-VMD-SVM, *Sensors*, **22**(16), 6281, (2022). https://doi.org/10.3390/s22166281

[7] Gunerkar RS, Jalan AK, Belgamwar SU. Fault diagnosis of rolling element bearing based on artificial neural net-work, *Journal of Mechanical Science and Technology*, **33**(2), 505-11, (2019). https://doi.org/10.1007/s12206-019-0103-x

[8] Liu Y, Xiang H, Jiang Z, Xiang J. Second-order transient-extracting S transform for fault feature extraction in rolling bearings, *Reliability Engineering and System Safety*, **230**, 108955, (2023). https://doi.org/10.1016/j.ress.2022.108955

[9] Liu Y, Xiang H, Jiang Z, Xiang J. Iterative Synchrosqueezing-Based General Linear Chirplet Transform for Time-Frequency Feature Extraction, *IEEE Transactions on Instrumentation and Measurement*, **72**, 3506711, (2023). https://doi.org/10.1109/TIM.2022.3232090

[10] Liu Y, Xiang H, Jiang Z, Xiang J. Refining the time-frequency characteristic of non-stationary signal for improving time-frequency representation under variable speeds, *Scientific Reports*, **13**(1), 5215, (2023). https://doi.org/10.1038/s41598-023-32333-w

[11] Wang L, Xiang J, Liu Y. A time-frequency-based maximum correlated kurtosis deconvolution approach for detecting bearing faults under variable speed conditions, *Measurement Science and Technology*, **30**(12), 125005, (2019). https://doi.org/10.1088/1361-6501/ab3678

[12] Fyfe KR, Munck E. Analysis of computed order tracking, *Mechanical Systems and Signal Processing*, **11**(2), 187-205, (1997). https://doi.org/10.1006/mssp.1996.0056

[13] Janssens O, Slavkovikj V, Vervisch B, et al.. Convolutional Neural Network Based Fault Detection for Rotating Machinery, *Journal of Sound and Vibration*, **377**, 331-345, (2016). https://doi.org/10.1016/j.jsv.2016.05.027

[14] Zhang W, Li C, Peng G, Chen Y, Zhang Z. A deep convolutional neural network with new training methods for bearing fault diagnosis under noisy environment and different working load, *Mechanical Systems and Signal Processing*, **100**, 439-453, (2018). https://doi.org/10.1016/j.ymssp.2017.06.022

[15] Zhao M, Zhong S, Fu X, Tang B, Pecht M. Deep Residual Shrinkage Networks for Fault Diagnosis, *IEEE Trans-actions on Industrial Informatics*, **16**(7), 4681-4690, (2020). https://doi.org/10.1109/TII.2019.2943898

[16] Zhi Z, Liu L, Liu D, Hu C. Fault Detection of the Harmonic Reducer Based on CNN-LSTM With a Novel Denoising Algorithm, *IEEE Sensors Journal*, **22**(3), 2572-2581, (2022). https://doi.org/10.1109/JSEN.2021.3137992

[17] Huang Y, Liao A, Hu D, Shi W, Zheng S. Multi-scale convolutional network with channel attention mechanism for rolling bearing fault diagnosis, *Measurement*, **203**, 111935, (2022). https://doi.org/10.1016/j.measurement.2022.111935

[18] Pan J, Zi Y, Chen J, Zhou Z, Wang B. LiftingNet: A Novel Deep Learning Network With Layerwise Feature Learning From Noisy Mechanical Data for Fault Classification, *IEEE Transactions on Industrial Electronics*, **65**(6), 4973-82, (2018). https://doi.org/10.1109/TIE.2017.2767540

[19] Zhao B, Zhang X, Zhan Z, Wu Q. Deep multi-scale adversarial network with attention : A novel domain adapta-tion method for intelligent fault diagnosis, *Journal of Manufacturing Systems*, **59**, 565-576, (2021). https://doi.org/10.1016/j.jmsy.2021.03.024

[20] Wang X, Mao D, Li X. Bearing fault diagnosis based on vibro-acoustic data fusion and 1D-CNN network, *Measurement*, **173**, 108518, (2021). https://doi.org/10.1016/j.measurement.2020.108518

[21] Liu X, Centeno J, Alvarado J, Tan L. One Dimensional Convolutional Neural Networks Using Sparse Wavelet Decomposition for Bearing Fault Diagnosis, *IEEE Access*, **10**, 86998-87007, (2022). https://doi.org/10.1109/ACCESS.2022.3199381

[22] Qi B, Li Y, Yao W, Li Z. Application of EMD Combined with Deep Learning and Knowledge Graph in Bearing Fault, *Journal of Signal Processing Systems for Signal Image and Video Technology*, **95**(8), 935-954, (2023). https://doi.org/10.1007/s11265-023-01845-z

[23] Hochreiter S, Schmidhuber J. Long short-term memory, *Neural Computation*, **9**(8), 1735-1780, (1997). https://doi.org/10.1162/neco.1997.9.8.1735

[24] Torres ME, Colominas MA, Schlotthauer G, Flandrin P, IEEE. A complete ensemble empirical mode decomposition with adaptive noise. 2011 IEEE International Conference on Acoustics, Speech and Signal Processing. *IEEE International Conference on Acoustics, Speech, and Signal Processing (ICASSP)*, 4144-4147, (2011). https://doi.org/10.1109/ICASSP.2011.5947265

[25] VAN DER Maaten L, Hinton G. Visualizing Data using t-SNE, *Journal of Machine Learning Research*, **9**, 2579-2605, (2008). `www.jmlr.org/papers/volume9/vandermaaten08a/vandermaaten08a.pdf`

[26] Song X, Cong Y, Song Y, Chen Y, Liang P. A bearing fault diagnosis model based on CNN with wide convolution kernels, *Journal of Ambient Intelligence and Humanized Computing*, **13**, 4041–4056, (2021). https://doi.org/10.1007/s12652-021-03177-x

[27] Zhang W, Peng G, Li C, Chen Y, Zhang Z. A New Deep Learning Model for Fault Diagnosis with Good Anti-Noise and Domain Adaptation Ability on Raw Vibration Signals, *Sensors*, **17**(2), 425, (2017). https://doi.org/10.3390/s17020425

[28] Zhao Z, Zhang Q, Yu X, et al.. Applications of Unsupervised Deep Transfer Learning to Intelligent Fault Diagnosis : A Survey and Comparative Study, *IEEE Transactions on Instrumentation and Measurement*, **70**, 3525828, (2021). https://doi.org/10.1109/TIM.2021.3116309

[29] He K, Zhang X, Ren S, Sun J. Deep Residual Learning for Image Recognition, *2016 IEEE Conference On Computer Vision and Pattern Recognition (Cvpr)*, 770-778, (2016). https://doi.org/10.1109/CVPR.2016.90